



Differential identification of GSH for acute coronary syndrome using a colorimetric sensor based on nanoflower-like artificial nanozymes

Dandan Zhang^{c,1}, Hongjin Zhang^{b,1}, He Sun^b, Yuanzhen Yang^d, Wenbin Zhong^b, Qing Chen^a, Qunxiang Ren^a, Ge Jin^{a,**}, Yang Zhang^{a,*}

^a School of Pharmacy, Shenyang Medical College, 146 Huanghe North Avenue, Shenyang, 110034, China

^b School of Basic Medicine, Shenyang Medical College, 146 Huanghe North Avenue, Shenyang, 110034, China

^c School of Public Health, Shenyang Medical College, 146 Huanghe North Avenue, Shenyang, 110034, China

^d School of Stomatology, Shenyang Medical College, 146 Huanghe North Avenue, Shenyang, 110034, China

ARTICLE INFO

Handling Editor: J. Wang

Keywords:

Nanozymes

Peroxidase

GSH

Colorimetric sensor

ABSTRACT

The ability to detect glutathione (GSH) concentrations in human blood offered a simple and non-invasive method to monitor changes associated with cardiovascular diseases, cancers and diabetes. We showed the potential of employing catalytically active protein-directed nanoflower-like artificial nanozymes (apo-TF-MnO_x NFs) by biomineralization method to produce simple and visible colorimetric sensor for GSH. The experiments proved that apo-TF-MnO_x NFs exhibited peroxidase, catalase- and superoxide dismutase-like activities, but the most notable feature was the excellent peroxidase-like activity, which could efficiently catalyze the oxidation reaction of 3,3',5,5'-tetramethylbenzidine (TMB) in the existence of hydrogen peroxide (H₂O₂) to generate a blue product. Some outcomes also indicated that the apo-TF-MnO_x NFs had stronger peroxidase-like activity, which was proved by the *Michaelis-Menten* constant (K_m) and maximum initial velocity (V_{max}). Hence, we used the peroxidase-like activity to develop a GSH colorimetric biosensor. Fortunately, the colorimetric platform exhibited a sensitive response to H₂O₂ and GSH in the range of 5 μM to 300 μM and 0.5 μM to 35 μM with a limit of detection of 3.29 μM and 0.15 μM (S/N = 3) under optimal conditions. The feasibility of the simple method was confirmed by qualitative detection of H₂O₂ and GSH in blood samples from acute coronary syndrome patients. A key outcome of our study was the ability to realized differential identification of GSH for acute coronary syndrome and healthy human without invasive treatment which was an advantage over other methods. This work not only proposed a new type of nanozymes, but also showed the multiple advantages of the apo-TF-MnO_x NFs for the construction of biosensors. Thus, we believe that apo-TF-MnO_x NFs with strong peroxidase-like activity can be employed as nanozymes and be widely applied in the fields of medicine and biological sensors.

1. Introduction

Nanozymes are a type of emerging material with unique physico-chemical features of nanomaterials and natural enzyme catalytic properties and have attracted great attention from scientists and the scholarly community in recent years [1–6]. In comparison to natural enzymes, they have unique and noteworthy advantages, such as high stability, alternative sources, tunable activity and low cost [7,8]. To date, emerging studies have unveiled that nanomaterials exhibit mimicking natural enzymes' properties, including carbon-based

nanomaterials [9,10], metal and metal oxide nanoparticles [11–13], noble metal nanoparticles [14,15], and various metal-organic frameworks (MOFs) [16–18]. These nanozymes have great potential to replace natural enzymes in the fields of biomedical analysis [19–21], environmental [22–24], food detection [25–27], disease treatment [28–30], and so on. Different, biosensors based on these nanozymes have been developed recently and popularized due to their superior advantages of convenient preparation and easy modification [31]. For example, Yang et al. prepared boron-doped Zn–N–C single-atom nanozymes and applied in the detection of p-phenylenediamine. In their study,

* Corresponding author.

** Corresponding author.

E-mail addresses: jinge1026@163.com (G. Jin), zhangyangpro@symc.edu.cn (Y. Zhang).

¹ Dandan Zhang and Hongjin Zhang contributed equally to this work.

single-atom nanozymes were applied for the first time as a potent peroxidase mimic, and showed satisfactory sensitivity and specificity with a wide response range and a low detection limit for p-phenylenediamine detection [32]. Our group developed a simple and facile colorimetric sensing strategy for GA and AA based on the manganese-based nanozymes [33]. However, in order to further investigate the general catalytic regularity and enhance sensitivity and convenience for detection, we still need to expand the research on the types of nanocomposites. Hence, exploiting new kinds of nanozyme mimics with high sensitivity to construct novel colorimetric sensors is an urgent demand.

Hydrogen peroxide (H_2O_2) is an essential molecule and an important reactive oxygen species in the living process, which can lead to severe damage for DNA and proteins. Different scholars have attested that many diseases, e.g., cardiovascular conditions, inflammatory cancer, and diabetes are related to the excess of H_2O_2 [34,35]. Glutathione (GSH), as a kind of key endogenous antioxidant, which can remove free radicals from the human body and considerably impact human health. The endogenous GSH content of healthy people is about 0.8–1.1 mM, and the oxidized glutathione (GSSG) level is often 0.10–0.15 mM [36]. The imbalance between GSH and GSSG is also concerned with some cardiovascular diseases, cancers and diabetes [37,38]. Therefore, the content of GSH and GSH/GSSG can be used as key indicators for these diseases. The scholarly community have reported a number of methods for determination of H_2O_2 and GSH levels, including optical and electrochemical sensing, which have important advantages such as high sensitivity and low detection limit. Nevertheless, these methods all need complex operations and sophisticated equipment. Among them, the colorimetric method can overcome disadvantages and offer important features such as high sensitivity, easy operation, and low costs, which make it easier for scientists to apply it for the detection of various substances, e.g., H_2O_2 , glucose, GSH, and autoantibodies. However, H_2O_2 and GSH colorimetric detection methods still give priority to natural

enzymes, such as horseradish peroxidase and glutathione reductase.

Here, a protein-directed apo-TF- MnO_x nanoflowers (NFs) by bio-mineralization method was proposed (Fig. 1A), and it was verified that the as-synthesized apo-TF- MnO_x NFs with small size (about 54.6 nm) display peroxidase-, catalase- and superoxide dismutase-mimic activities. What caught our attention the most was the excellent peroxidase-like activity that shows the potential of these nanozymes to be a substitute of natural enzymes in the construction of sensitive colorimetric sensor for detecting H_2O_2 and GSH. More significantly, the K_m and the V_{max} value were calculated using the *Michaelis-Menten* equation and the results support this conclusion. The proposed sensors showed high sensitivity, low limit of detection, and credible repeatability in the blood samples from acute coronary syndrome patients and achieved differential detection. Hence, we believe that our results can be used as examples of the successful medical application of nanozymes.

2. Experimental section

2.1. Chemicals and materials

Apo-transferrin (Apo-TF), hydroethidine (HE), GSH and terephthalic acid (TA) were purchased from Sigma-Aldrich. Manganese chloride tetrahydrate ($MnCl_2 \cdot 4H_2O$), sodium hydroxide (NaOH), hydrogen peroxide (H_2O_2 , 30%) and analytically purity grade salts used for preparation of buffers were purchased from Sinopharm Chemical Reagent Co. Ltd. (China). 3,3,5,5-tetramethylbenzidine (TMB) used in the experiments was from TCI (Shanghai, China). The ultrapure water (18.0 M Ω cm) was used throughout the whole experiment. Human whole blood samples from five patients with acute coronary syndrome and healthy human volunteers were provided by the affiliated hospital of Qingdao University.

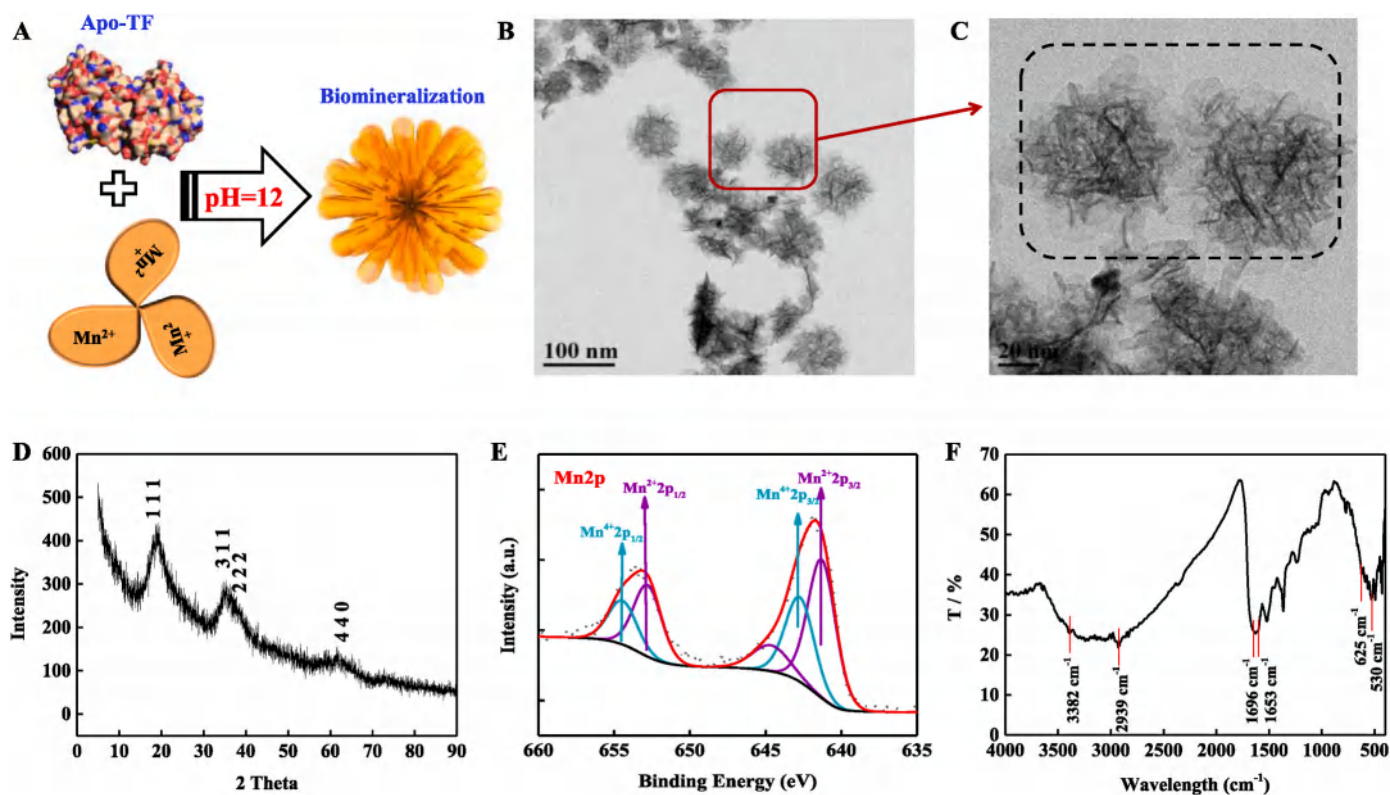


Fig. 1. Apo-TF-directed synthesis and characterization of apo-TF- MnO_x NFs. (A) Synthesis schematic of apo-TF- MnO_x NFs; (B, C) TEM images of apo-TF- MnO_x NFs with the different magnification; (D) XRD pattern of apo-TF- MnO_x NFs; (E) High-resolution XPS Mn 2p spectra of apo-TF- MnO_x NFs. (F) FT-IR spectra of apo-TF- MnO_x NFs.

2.2. Synthesis of apo-TF-MnO_x NFs

Apo-TF-MnO_x NFs were synthesized by improved biomineralization method. Briefly, 10 mg Apo-TF was dissolved into MnCl₂·4H₂O aqueous solution (10 mL, 5.85 × 10⁻³ M), then the mixture solutions were continuously stirred for 30 min at room temperature. Subsequently, 1 M NaOH was added to adjust the pH to 12, and the whole biomineralization process lasted 2 h. The obtained products were dialyzed for 24 h to eliminate extra ions and free Apo-TF, centrifuged (1.2 × 10⁴ rpm) and stored at 4 °C after freeze drying.

2.3. Enzymatic activity analysis

The peroxidase activity analysis of apo-TF-MnO_x NFs depended on colorimetric reaction. TMB could change into oxTMB, achieving the color reaction and salient absorption peak at 652 nm when the catalysis of materials happened. Typically, apo-TF-MnO_x NFs (50 μg mL⁻¹) performed peroxidase-like activity in the adjusted buffer solution containing H₂O₂ (1 mM) and TMB (0.5 mM). After incubated for 10 min at room temperature, the absorbance spectrum of oxTMB ($\epsilon_{650\text{ nm}} = 39\,000\text{ m}^{-1}\text{ cm}^{-1}$) was measured at 652 nm by a microplate reader. Then, the pH, temperature or incubation time effects on the peroxidase-like catalytic activity were analyzed to determine the optimum conditions following the above assay. The adjusted pH ranged from 1 to 10, and the temperature was optimized from 25 to 65 °C.

Subsequently, we evaluated the CAT-mimic activity of apo-TF-MnO_x NFs, depending on the produced oxygen content (unit: mg L⁻¹) at indoor temperature. In detail, 50 μL apo-TF-MnO_x NFs (1 mg mL⁻¹) and 100 μL H₂O₂ were added into the buffer solution (pH 7.0), maintaining the total volume at 2 mL, then keeping a record of generated O₂ solubility. We employed a commercial colorimetric SOD assay kit (S311-10) to evaluate the superoxide dismutase (SOD)-like activity of apo-TF-MnO_x NFs, and strictly followed the instructions to perform actions at room temperature. The SOD-like activities of apo-TF-MnO_x NFs with different concentration were showed as the inhibition ratio of the competitive WST reaction with superoxide by natural SOD enzyme.

Furthermore, we investigated the kinetics of the catalytic reaction by monitoring the changes of absorbance at 652 nm, as the initial concentration of either TMB (0.2–3 mM) or H₂O₂ (0.05–2 mM) was pre-established under the aforementioned optimized conditions (pH = 4, T = 37 °C). The typical *Michaelis-Menten* curves were obtained at a certain concentration range of TMB or H₂O₂, and the *Michaelis* constant (K_m) and maximum velocity (V_{max}) were analyzed using the *Lineweaver-Burk* double reciprocal plot for inquiring the mechanism of proposed catalytic process of apo-TF-MnO_x NFs. The equation of apparent kinetic parameters used during the procedures was as follows:

$$V = (V_{\text{max}} * [S]) / (K_m + [S])$$

where V is the reaction velocity, V_{max} is maximal reaction velocity, $[S]$ is the concentration of substrate and K_m is the *Michaelis* constant. K_m represents the affinity of the nanozyme with its substrate. The peroxidase-mimicking catalytic efficiency is defined by k_{cat}/K_m , where k_{cat} is the catalytic constant, $k_{\text{cat}} = V_{\text{max}}/[E]$.

Terephthalic acid (TA) was selected to capture the hydroxyl radicals for catalytic oxidation reaction, and generated 2-hydroxy terephthalic acid presented intensity fluorescence with the emission wavelength at 435 nm. Typically, apo-TF-MnO_x NFs (50 μg mL⁻¹), TA (0.5 mM), H₂O₂ (2 mM) were added to the acetate buffer (0.1 M, pH = 4) for 30 min at 37 °C. Fluorescence spectrum was analyzed with an excitation wavelength of 315 nm.

2.4. Colorimetric detection of H₂O₂ and GSH

The detection of H₂O₂ was carried out according to the following steps: (i) different concentrations of 100 μL H₂O₂ solution (10 μM–1000

μM) was added into the buffer solution (pH = 5) consisting of apo-TF-MnO_x NFs (100 μg mL⁻¹) and TMB (1 mM) to maintain the total volume at 2 mL, and (ii) the above mixed system reacted for 10 min, and the absorbance at 652 nm was recorded. All experiments were performed in parallel three times.

The detection of GSH was performed by added 400 μL GSH with various concentrations into 5 mM sodium citrate buffer solution (pH 4.0) containing 0.2 mM H₂O₂, 0.2 mM TMB and 100 μg mL⁻¹ apo-TF-MnO_x NFs. The mixture was kept at 37 °C for 20 min. Solution treatment and determination methods abided by the steps of H₂O₂ detection mentioned above.

2.5. Preparation of real samples

The method of McDermott et al. [39] was followed for collecting and processing blood samples. Noticing that the perchloric acid could oxidize GSH in the adsorption process, we used TCA instead of perchloric acid. In detail, the human whole blood samples were prepared for the detection of GSH and H₂O₂. 1.0 mL of these samples was added into 1.0 mL of trichloroacetic acid, then the mixture experienced vortex for 30 s, following a complete cooling process for 10 min on the as-prepared ice for precipitating proteins. Finally, the mixture was centrifuged at 13 000 rpm, and the supernatant fluid was determined according to the steps mentioned in section 2.4 for real blood sample analysis.

3. Results and discussion

3.1. Synthesis and characterization of apo-TF-MnO_x NFs

The nanoflower-like apo-TF-MnO_x NFs was successfully synthesized using the proposed biomineralization method and the synthetic procedure is presented in Fig. 1A. Apo-TF was chosen as template, which enhanced the stability and dispersion of apo-TF-MnO_x NFs. As shown in Fig. 1B and C, the nanoflower-like morphology of the as-prepared apo-TF-MnO_x NFs was observed using TEM, and showed good monodispersity and a uniform size of about 54.6 nm. The dynamic light scattering (DLS) result was consistent with the TEM (Fig. S1), demonstrating that there were no obvious hydration layers generated on the surface of apo-TF-MnO_x NFs. The UV absorption spectrum exhibited a typical absorption peak of apo-TF at 282 nm and manganese oxide at 382 nm, indicating the successful prepared of apo-TF-MnO_x NFs (Fig. S2). XRD pattern of apo-TF-MnO_x NFs was shown in Fig. 1D, all the measured diffraction peaks were well matched to the crystal faces of (1 1 1) (3 1 1), (2 2 2) and (4 4 0) of Mn₃O₄ from standard spectrum (PDF#13-0162), displayed their highly crystalline nature. XPS was executed to analyze the chemical valence and binding of the element. In Figs. S3 and C, O, N, S and Mn elements were all observed in the full survey XPS spectrum of apo-TF-MnO_x NFs. The high-resolution XPS Mn 2p spectrum showed two chemical states: Mn(II) characterized by 2p_{3/2} with binding energies of 641.3 and 652.8 eV, and Mn(IV) characterized by 2p_{3/2} with binding energies of 642.7 and 654.5 eV (Fig. 1E). These results illustrated the multivalences of Mn of apo-TF-MnO_x NFs and we noted MnO_x. Besides, the C 1s spectrum exhibited three peaks respectively centered at 287.8, 285.1 and 284.4 eV, which corresponded to C–O, C–N, and C–C groups (Fig. S4). The high-resolution XPS of N 1s (Fig. S5A), O 1s (Fig. S5B) and S 2p (Fig. S5C) exhibited distinct bulge peaks, respectively, indicating the existence of apo-TF. Apo-TF-MnO_x NFs surface chemistry was confirmed by FT-IR in Fig. 1F, the results showed that typical amide I band peak around 1696 cm⁻¹ and amide II band peak around 1653 cm⁻¹, and the peaks at about 625 cm⁻¹ and 530 cm⁻¹ were typical Mn–O absorption bands. Our outcomes confirm the successful synthesis process of apo-TF-MnO_x NFs nanoflowers.

3.2. Multi-enzyme-like activity of apo-TF-MnO_x NFs

Based on the successful construction of apo-TF-MnO_x NFs, the multiple enzyme-like properties were explored by catalytic oxidation of a series of typical substrates. First, the POD-like activities of as-prepared apo-TF-MnO_x NFs were evaluated using TMB as typical chromogenic substrates (Fig. 2A). In order to distinguish oxidase activity the whole experiment was performed in a nitrogen atmosphere (Fig. 2C). As expected, apo-TF-MnO_x NFs could catalyze oxidation of colorless TMB and turned into blue oxidized TMB (oxTMB) in the presence of H₂O₂. The maximum absorbance of the mixture was centered at 652 nm, a result that is due to the charge-transfer complexes derived from the one-electron oxidation of TMB [40]. Negligible absorbance was observed in the control groups, indicating that apo-TF-MnO_x NFs played a catalytic role in the oxidation process of TMB (Fig. 2B). As shown in Fig. 2D, we also explored the CAT-mimic activity of apo-TF-MnO_x NFs. We confirm apo-TF-MnO_x NFs could catalyze H₂O₂ to decompose to generate O₂, and we chose a dissolved oxygen meter to test O₂ generation with a series of concentration of H₂O₂ at an optimal pH (pH = 6.0) (Fig. S6A) and reaction time (Fig. S6B). These results illustrated that prepared apo-TF-MnO_x NFs had CAT-like activity. Moreover, a commercialized SOD-assay was used to evaluate SOD-mimic activity of apo-TF-MnO_x NFs. During the procedure, water-soluble WST-1 reacted with superoxide anion radicals (O₂^{•-}) to generate WST-1 formazan. Strikingly, the generation of the reaction process was inhibited by the SOD or the analogue with SOD-like activity. Apo-TF-MnO_x NFs with different concentrations was added to investigate the SOD-like performance, which depended on the ratio inhibition of the competitive WST reaction with O₂^{•-} by natural SOD enzyme. As shown in Fig. 2E, as the concentration of apo-TF-MnO_x NFs kept increasing, the inhibition effect became more evident, indicating the presence of SOD-mimic activity.

Our results prove that apo-TF-MnO_x NFs have impressive POD-like, CAT-like and SOD-like catalytic activity, which could act as a potential alternative to multiple kinds of natural enzymes and be applied in many fields. In this work, we mainly discussed POD-like and catalytic mechanism, but there is room to explore the potential of other features confirmed by our experiments.

Similar to general peroxidase-like nanomaterials, the peroxidase-like activity of apo-TF-MnO_x NFs was also affected by pH, temperature, and reaction time. As illustrated in Fig. 3, apo-TF-MnO_x NFs showed a high catalytic activity over pH (Fig. 3A) ranging from 2.5 to 6.0 and a broad range of temperature going from 25 to 65 °C (Fig. 3B). Based on the study of experimental conditions, the optimal reaction conditions for apo-TF-MnO_x NFs were 45 °C of temperature and a pH 4.0, indicating the presence of a relatively high peroxidase-like activity even in acidic condition and a higher temperature. H₂O₂ was squinted toward decomposition at alkaline conditions and high temperatures, resulting in the decrease of H₂O₂ reaction in the catalytic system.

3.3. Catalytic mechanism and kinetic assay of peroxidase-like mimics

The catalytic mechanism and enzyme activity of apo-TF-MnO_x NFs were investigated by selected hydroethidine (HE) and terephthalic acid (TA) as fluorescence probe, which could track $\bullet\text{O}_2^-$ and $\bullet\text{OH}$ to generate ethidium and 2-hydroxyterephthalic acid and with strong fluorescence emission at around 590 nm and 425 nm [41].

As a result, there was no obvious change of fluorescence at 590 nm with the increased concentration of apo-TF-MnO_x NFs, proving that $\bullet\text{O}_2^-$ was not generated (Fig. 4A). However, apo-TF-MnO_x NFs catalyzed H₂O₂ and TA to produce the stronger fluorescence intensity under the same concentration and time (Fig. 4B). The results proved the existence of $\bullet\text{OH}$ in the catalytic process and it has also further demonstrated that

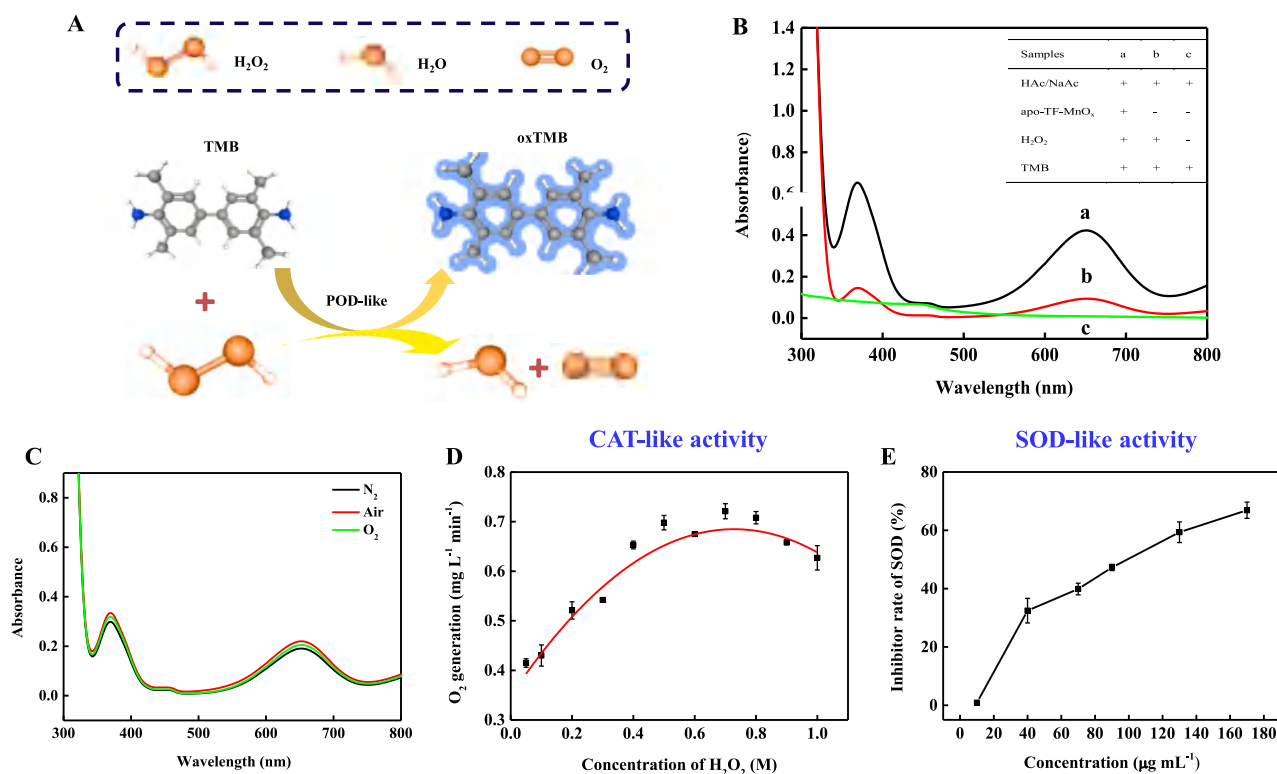


Fig. 2. (A) Schematic illustration of the POD-like of apo-TF-MnO_x NFs. (B) POD-like activity: typical absorption spectra of TMB, oxidation catalyzed by apo-TF-MnO_x NFs and control groups in the presence of H₂O₂ at pH 4.0. (C) Absorbance spectra of TMB oxidation based on POD-like activity in a N₂, Air, and O₂ atmosphere. (D) CAT-like activity: oxygen generation catalysis by apo-TF-MnO_x NFs (80 μg mL⁻¹) with a series of concentration of H₂O₂ at pH 6.5. (E) SOD-like activity: inhibitor rate of SOD on a series of concentration of apo-TF-MnO_x NFs at pH 8.0. Error bars represent the standard error derived from three repetitive measurements.

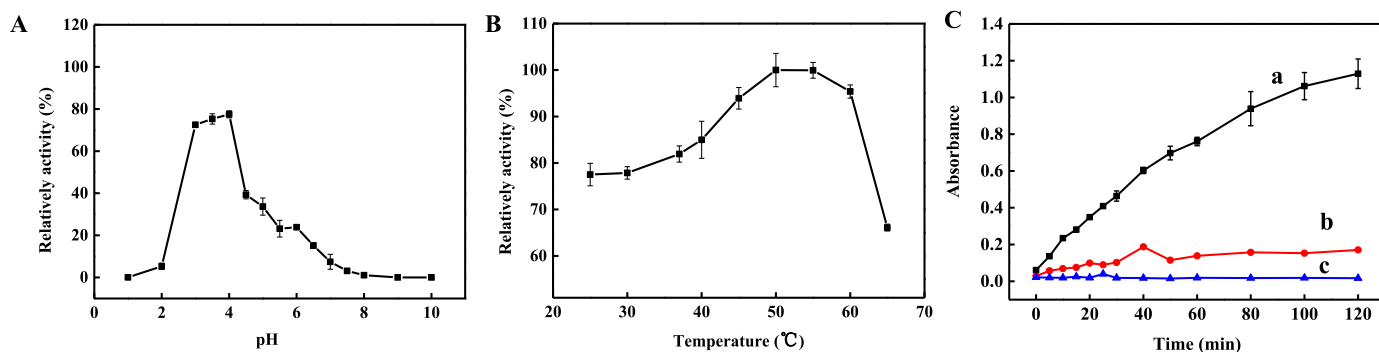


Fig. 3. The effect of pH (1–10) (A), temperature (25 °C–65 °C) (B) on the peroxidase-like activity of apo-TF-MnO_x NFs. (C) Time-dependent absorbance of TMB aqueous solution in different reaction systems: (a) apo-TF-MnO_x NFs + H₂O₂ + TMB; (b) H₂O₂ + TMB; (c) TMB.

apo-TF-MnO_x NFs has peroxidase activity. Furthermore, we also identified that the fluorescent intensity increased as the concentration of apo-TF-MnO_x NFs surged, indicating that the as-prepared apo-TF-MnO_x NFs were capable of decomposing H₂O₂ into •OH by absorbing H₂O₂ on the surface of the nanocomposite. Besides, the nanocomposites could also stabilize the generated •OH to catalyze the oxidation reaction of TMB to form a blue product, and then accelerate the catalytic reaction process. The catalytic reaction speeds of apo-TF-MnO_x NFs surged with the substrate concentrations increasing gradually until up to a plateau, demonstrating the catalytic reaction followed the *Michaelis-Menten* kinetics (Fig. 4C and D). According to the Line weaver-Burk plot, the *Michaelis-Menten* constant (K_m) was calculated to be 6.29 μM for H₂O₂ substrate (Figs. 4E) and 0.18 mM for TMB substrate (Fig. 4F). The lower K_m value of apo-TF-MnO_x NFs indicated a higher affinity between apo-TF-MnO_x NFs and the substrate.

3.4. Colorimetric detection of H₂O₂ and GSH based on apo-TF-MnO_x NFs

To quantitative detection of H₂O₂, a simple and effective colorimetric sensor was employed based on the apo-TF-MnO_x NFs. As displayed in Fig. S7, with the rise of the concentration of H₂O₂, the corresponding absorbance increased gradually with the absorbance value at 652 nm, and exhibited a good linear correlation ($R^2 = 0.9906$) and concentration of H₂O₂ in the wide range of 5.0–300 μM with a limit of detection (LOD) of 3.29 μM (LOD = 3s/k, where s represents the relative standard deviation, k is the slope of the linear calibration plots).

GSH acts as an original antioxidant capable of promoting oxTMB reduction, and TMB can be catalyzed to oxTMB by apo-TF-MnO_x NFs in the presence of H₂O₂. However, as GSH was added, the color of the mixture gradually lightens until it becomes colorless. Inspire of this principle, a facile colorimetric sensor was employed for the determination of GSH. The sensitivity of the GSH sensor was investigated by adding a series of concentrations of GSH under the above optimal conditions (Fig. 5A). As results, the more GSH concentration was added, the weaker light absorption intensity at 652 nm was showed, and the decrease of absorbance and the concentration of GSH exhibited a favourable linear relationship ranging from 0.5 to 25 μM ($\Delta A = 32.309$ [GSH] − 0.001, $R^2 = 0.9956$) and 25–35 μM ($\Delta A = 3.0747$ [GSH] + 0.7425, $R^2 = 0.9942$) (Fig. 5B). The detection limit of GSH was up to 0.15 μM (3s/k), which is superior to the numbers presented in previous reports (Table S1). Moreover, with the addition of GSH, the color changed clearly and easy distinguished by naked eyes. Significantly, a simple sensing platform based on apo-TF-MnO_x NFs was provided for the visual detection of GSH. To consider the practicability of proposed colorimetric biosensor in complex samples, the anti-interference capability of this sensing platform was assessed by examining possible interfering substances, including common cations (Na⁺, K⁺ and Ca²⁺), and conventional amino acids [cysteine (Cys), tyrosine (Tyr), Phenylalanine (Phe), Lysine (Lys), L-Aspartic Acid (Asp) and Histidine (His)],

glucose (Glu) and dopamine (DA). The colorimetric results showed that there was no evident interference signal whether individual substances or mixtures except Cys (Fig. 5C). Fortunately, the contents of Cys were much lower than GSH in real biological samples, and the effect of Cys also inhibited the oxidation of TMB, which could play a synergistic effect with GSH. Hence, the selectivity of the sensing platform was acceptable. In addition, we confirmed that the apo-TF-MnO_x NFs have high stability and showed no obvious aggregation in aqueous solution for 30 days (Fig. 5D) and POD-like activities were still kept over 80%, elucidating the splendid reliability and stability of apo-TF-MnO_x NFs nanozyme.

3.5. Analysis of whole blood samples

To further estimate the performance of this proposed assay method in real samples with the complicated matrix, specifically whole blood from patients with acute coronary syndrome and healthy people were selected as model samples to quantitatively detect GSH and GSSG. After determining the level of GSH, the blood sample was experienced by sodium borohydride, the GSSG was reduced to GSH, and then we determined the total content of GSH and GSSH. The results were illustrated in Fig. 6 A and B. The detected amount of GSH and GSSG in healthy people was in accordance with the results previously reported in related studies [38]. However, the amounts of GSH displayed a decrease for patients with acute coronary syndrome, but the content of GSSH increased. Therefore, neither the total amounts of GSH nor the GSSG levels could be used to clearly distinguish acute coronary syndrome patients and healthy people. Differently, the GSH/GSSG levels could be used as parameters to distinguish between healthy people and diagnosed patients (Fig. 6C), proving the high application value of the biosensor. To consider the veracity of this colorimetric biosensor, the content of H₂O₂ and GSH in the blood of healthy people was measured by the spike-recovery test. A series of H₂O₂ and GSH with different concentrations were introduced into these blood samples by standard addition method. Notably, the recovery rates of H₂O₂ ranged from 90.8% to 110.4% and the relative standard deviation (RSD) values were lower than 4.2% (Table S2). Also, the recovery rates of GSH ranged from 86.3% to 115.8% and the RSD values were lower than 3.9% (Table 1), which demonstrated that the colorimetric H₂O₂ and GSH sensor were suitable for real samples.

4. Conclusions

In summary, the apo-TF-MnO_x NFs were prepared successfully by bio-mineralization method and exhibited excellent peroxidase-like activity. Our results proved that the catalytic reaction of apo-TF-MnO_x NFs was based on the •OH. Based on the excellent peroxidase-like performance, a simple and facile platform for colorimetric detection of H₂O₂ and GSH was successfully proposed, the linear range of H₂O₂ was from 5 μM to 300 μM and the detection limit could reach as low as 3.29 μM. As

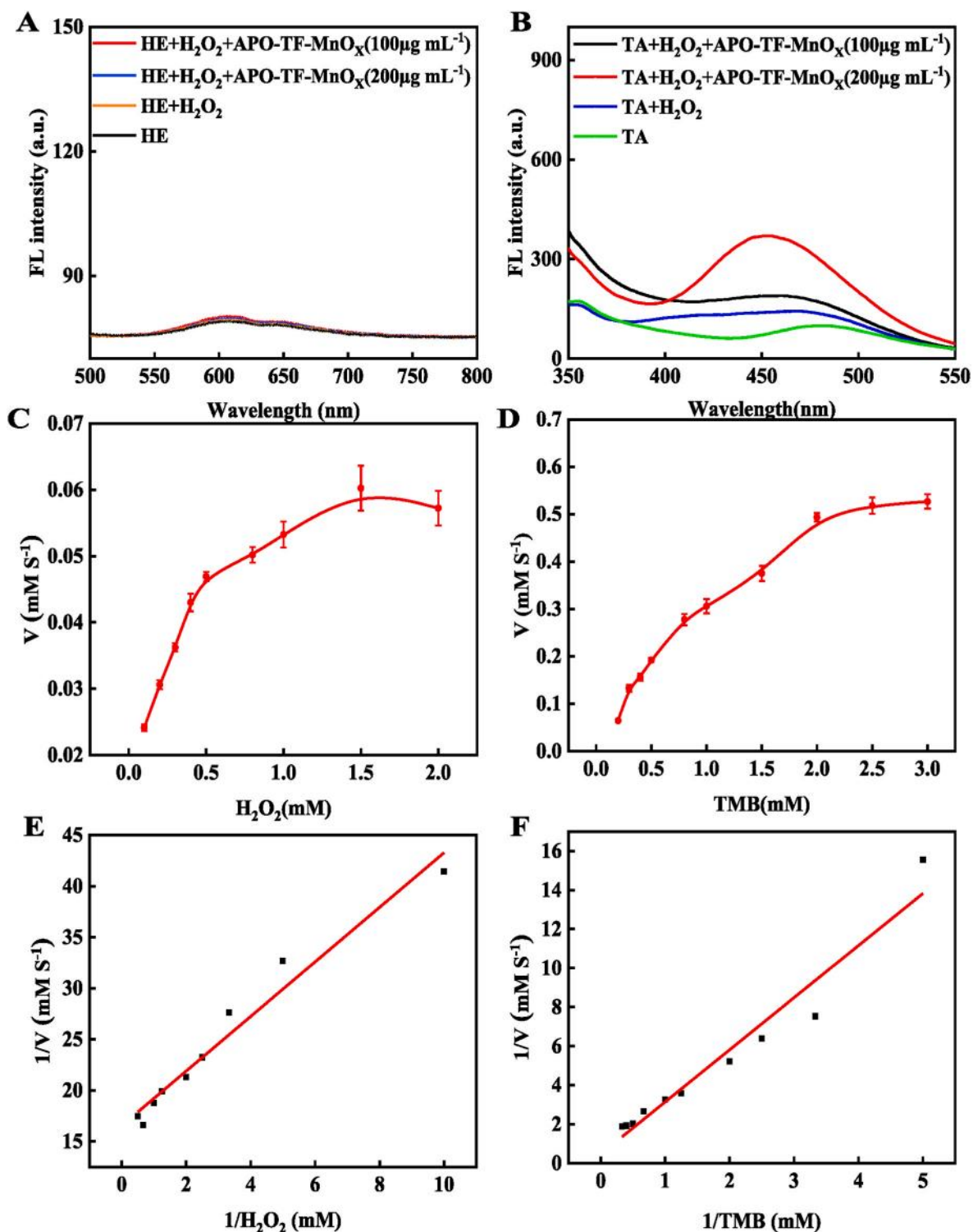


Fig. 4. Fluorescent spectra of HE (A) and TA (B) after reaction with H₂O₂ in the absence and presence of apo-TF-MnO_x NFs. Characterization of the catalytic kinetics of POD. *Michaelis-Menten curves* for apo-TF-MnO_x NFs. The steady-state kinetic assay of apo-TF-MnO_x NFs. (C) The concentration of TMB was 2 mM and the H₂O₂ concentration varied. (D) The concentration of H₂O₂ was 1 M and the TMB concentration varied. (E, F) Double reciprocal plots of the *Michaelis-Menten* equation from the activity data of the concentration of H₂O₂ and TMB.

for GSH, the linear range was from 0.5 μ M to 35 μ M, and the LOD was 0.15 μ M, which was far below the permissible level in human blood samples. Therefore, the constructed colorimetric sensor was well applied to the detection of GSH in blood samples of acute coronary syndrome patients. Encouragingly, the proposed colorimetric sensor achieved differential determination between acute coronary syndrome

patients and healthy people. We expect that this novel sensor can be further applied in disease detection and treatment involving other types of medical conditions and diagnoses.

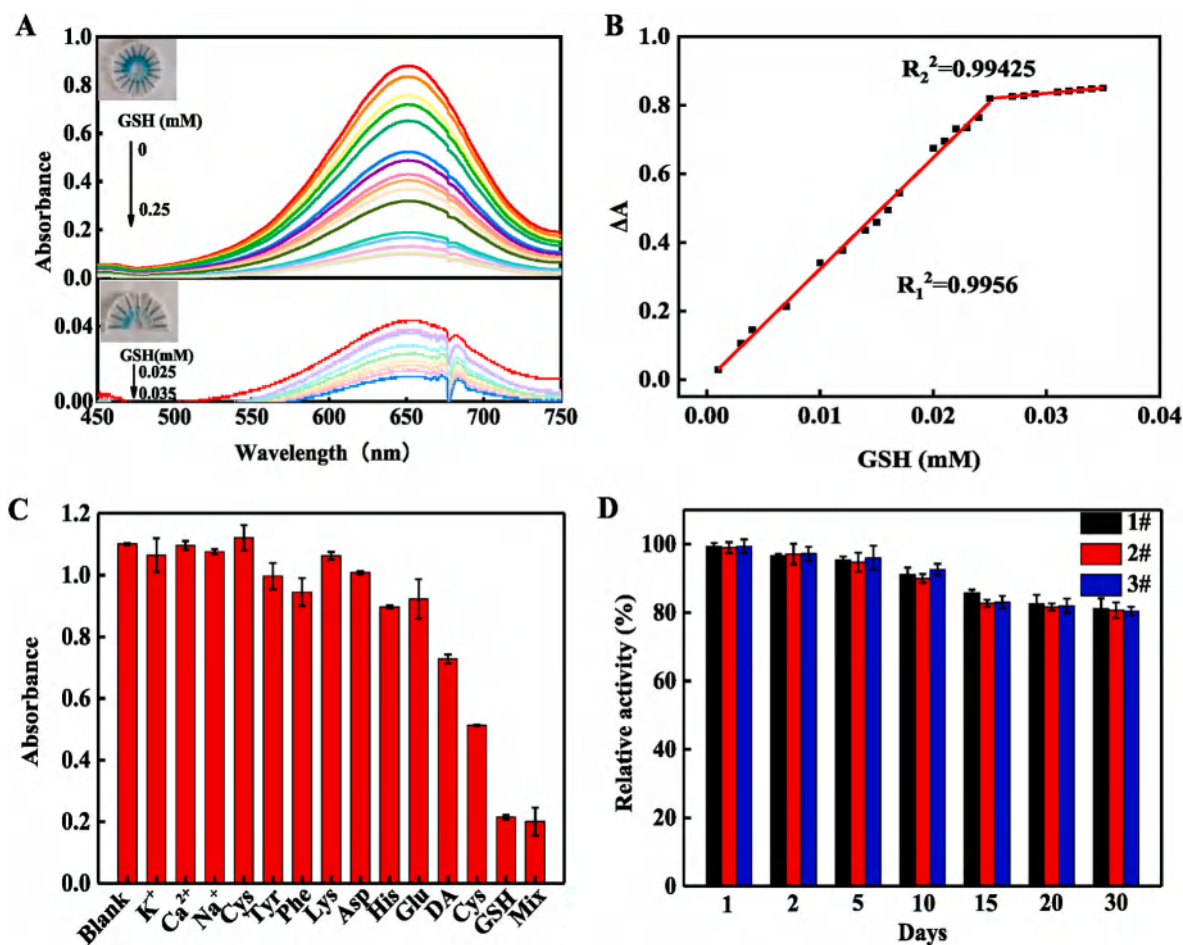


Fig. 5. (A) UV-Vis absorbance curves of apo-TF-MnO_x NFs (50 μg mL⁻¹), TMB (0.5 mM) and H₂O₂ (5 mM) at various concentrations of GSH. Inset: Color change of reaction system under different concentrations of GSH. (B) The linear calibration plots for the quantitative determination of GSH ($\Delta A = A_0 - A$, where A_0 and A are the absorbance of the reaction system without and with GSH). (C) Absorbance value of the reaction system toward GSH and other interfering species. [GSH] = 80 μM. The concentration of K⁺, Ca²⁺, Na⁺ is 400 μM, and other interfering species are 160 μM. (D) The stability and repeatability of POD-like activities for apo-TF-MnO_x NFs at optimal conditions within 30 days. 1#, 2# and 3# represent three parallel experiments.

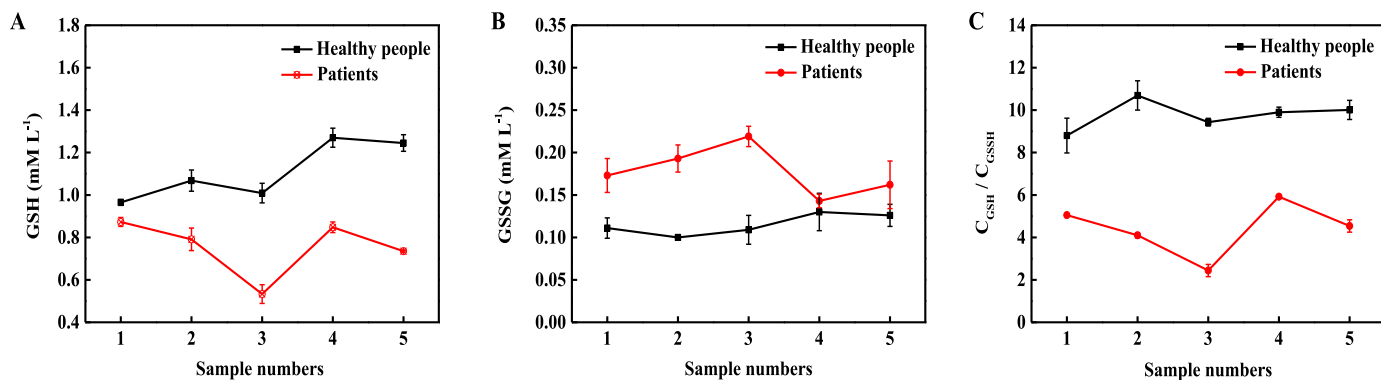


Fig. 6. Content of GSH (A), GSSG (B) and GSH/GSSG (C) in human blood of five healthy people and five patients with acute coronary syndrome determined by our proposed GSH sensor.

Credit author statement

Dandan Zhang: Validation, Writing-review and editing, Funding acquisition. Hongjin Zhang: Writing-review and editing, Software, Investigation. He Sun: Investigation. Yuanzhen Yang: Investigation. Wenbin Zhong: Investigation. Qing Chen: Investigation. Qunxiang Ren: Supervision, Investigation. Ge Jin: Supervision, Investigation, Writing-

review and editing. Yang Zhang: Conceptualization, Methodology, Investigation, Writing-original draft, Project administration, Funding acquisition.

Declaration of competing interest

The authors declare no competing financial interest.

Table 1

Recovery test for determination of GSH in five human whole blood (n = 3).

Sample	GSH (mM)	Added (mM)	Founded (mM)	Recovery (%)	RSD (%)
1#	0.89	0.50	1.20	86.3	1.4
		1.00	1.74	92.1	2.4
		1.50	2.24	93.7	0.5
2#	1.12	0.50	1.69	104.3	1.8
		1.00	2.22	104.7	2.6
		1.50	2.47	94.3	3.9
3#	0.96	0.50	1.54	105.5	2.9
		1.00	2.27	115.8	2.2
		1.50	2.34	95.1	0.7
4#	1.09	0.50	1.39	87.4	3.0
		1.00	1.99	95.2	1.4
		1.50	2.68	103.5	0.9
5#	1.23	0.50	1.52	87.9	1.2
		1.00	2.01	90.1	2.5
		1.50	2.88	105.5	3.8

Data availability

No data was used for the research described in the article.

Acknowledgments

The authors appreciate Science Research Foundation of Education Department for Liaoning Province (LJKMZ20221790 and SYXX202005), National Natural Science Foundation of China (No. 21804093), PhD Start-up Foundation of Liaoning Province (2021-BS-284).

Appendix A. Supplementary data

Supplementary data to this article can be found online at <https://doi.org/10.1016/j.talanta.2023.124967>.

References

- X. Cui, G.H. Lu, F. Fang, Y. Xiong, S. Tian, Y.P. Wan, Y.F. Xiao, D. Shen, H. Wang, J. F. Zhang, C.S. Lee, Iron self-boosting polymer nanoenzyme for low-temperature photothermal-enhanced ferrotherapy, *ACS Appl. Mater. Interfaces* 13 (2021) 30274–30283.
- Y.Y. Huang, J.S. Ren, X.G. Qu, Nanozymes: classification, catalytic mechanisms, activity regulation, and applications, *Chem. Rev.* 119 (2019) 4357–4412.
- Y.C. Li, L.L. Wang, Z.W. Cui, S.J. Liu, S.C. Wang, J. Ren, Y.L. Tian, R. Shu, X. Luo, Y.J. Liao, J.L. Wang, D.H. Zhang, White peroxidase-mimicking nanozyme-nanocarrier of enzyme labeled antibody to enhance catalytic performance and relieve color interference of immunoassay, *Sens. Actuata. B Chem.* 364 (2022), 131909.
- X.Y. Zhu, T. Li, X. Hai, S. Bi, A nanozyme-based colorimetric sensor array as electronic tongue for thiols discrimination and disease identification, *Biosens. Bioelectron.* 213 (2022), 114438.
- X.Y. Zhang, X.Y. Zhu, Y.F. Li, X. Hai, S. Bi, A colorimetric and photothermal dual-mode biosensing platform based on nanozyme-functionalized flower-like DNA structures for tumor-derived exosome detection, *Talanta* 258 (2023), 124456.
- X. Hai, Y.W. Li, K.X. Yu, S.Z. Yue, Y.F. Li, W.L. Song, S. Bi, X.J. Zhang, Synergistic in-situ growth of silver nanoparticles with nanozyme activity for dual-mode biosensing and cancer theranostics, *Chin. Chem. Lett.* 32 (2021) 1215–1219.
- P. Mishra, J.S. Lee, D. Kumar, R.O. Lauro, N. Costa, D. Pathania, S. Kumar, J. Lee, L. Singh, Engineered nanozymes with multifunctional properties for next-generation biological and environmental applications, *Adv. Funct. Mater.* 32 (2022), 2108650.
- X.N. Liu, L.J. Huang, Y.P. Wang, J. Sun, T.L. Yue, W.T. Zhang, J.L. Wang, One-pot bottom-up fabrication of a 2D/2D heterojunction nanozyme towards localized peroxidase-like activity for sulfide ions sensing, *Sens. Actuata. B Chem.* 306 (2020), 127565.
- Q. Xu, H. Yuan, X.L. Dong, Y. Zhang, M. Asif, Z.H. Dong, W.S. He, J.H. Ren, Y. M. Sun, F. Xiao, Dual nanozymes modified microelectrode based on carbon fiber coated with AuPd alloy nanoparticles decorated graphene quantum dots assembly for electrochemical detection in clinic cancer samples, *Biosens. Bioelectron.* 107 (2018) 153–162.
- C.Y. Chen, Y.Z. Tan, P.H. Hsieh, C.M. Wang, H. Shibata, K. Maejima, T.Y. Wang, Y. Hiruta, D. Citterio, W.S. Liao, Metal-free colorimetric detection of pyrophosphate ions by inhibitive nanozymatic carbon dots, *ACS Sens.* 5 (2020) 1314–1324.
- G.N. Huang, J.K. Zang, L.Z. He, H.L. Zhu, J.R. Huang, Z.W. Yuan, T.F. Chen, A. D. Xu, Bioactive nanozymes reverses oxidative damage and endoplasmic reticulum stress in neurons under ischemic stroke, *ACS Nano* 16 (2022) 431–452.
- L. Wang, J.J. Hou, S.Z. Li, A.J. Carrier, Q.S. Liang, D. Oakley, X. Zhang, CuO nanoparticles as haloperoxidase-mimics: chloride-accelerated heterogeneous Cu-fenton chemistry for H₂O₂ and glucose sensing, *Sens. Actuata. B-Chem* 287 (2019) 180–184.
- W.X. Du, T.Z. Liu, F.F. Xue, X.J. Cai, Q. Chen, Y.Y. Zheng, H.R. Chen, Fe₃O₄ mesocrystals with distinctive magnetothermal and nanozymes activity enabling self-reinforcing synergistic cancer therapy, *ACS Appl. Mater. Interfaces* 12 (2020) 19285–19294.
- Y.J. Zhan, Y.B. Zeng, L. Li, L.H. Guo, F. Luo, B. Qiu, Y.J. Huang, Z.Y. Lin, Cu²⁺-modified boron nitride nanosheets-supported subnanometer gold nanoparticles: an oxidase-mimicking nanozymes with unexpected oxidation properties, *Anal. Chem.* 92 (2020) 1236–1244.
- Z.L. Tan, H. Dong, Q. Liu, H. Liu, P.P. Zhao, P. Wang, Y.Y. Li, D.P. Zhang, Z. D. Zhao, Y.H. Dong, A label-free immunosensor based on PtPd NCS@MoS₂ nanozymes for hepatitis B surface antigen detection, *Biosens. Bioelectron.* 142 (2019), 111556.
- J.T. Liu, L.Y. Ye, W.H. Xiong, T.R. Liu, H. Yang, J.P. Lei, A cerium oxide@metal-organic framework nanozymes as a tandem catalyst for enhanced photodynamic therapy, *Chem. Commun.* 57 (2021) 2820–2823.
- D.D. Wang, H.H. Wu, W.Q. Lim, S.Z.F. Phua, P.P. Xu, Q.W. Chen, Z. Guo, Y.L. Zhao, A mesoporous nanozymes derived from metal-organic frameworks with endogenous oxygen generation to alleviate tumor hypoxia for significantly enhanced photodynamic therapy, *Adv. Mater.* 31 (2019), 1901893.
- C. Li, C.J. Liu, R. Liu, Y.X. Wang, A.Y. Li, S. Tian, W. Cheng, S.J. Ding, W.T. Li, M. Zhao, Q.F. Xia, A novel CRISPR/Cas14a-based electrochemical biosensor for ultrasensitive detection of burkholderia pseudomallei with PtPd@PCN-224 nanozymes for signal amplification, *Biosens. Bioelectron.* 225 (2023), 115098.
- X.D. Zhang, X.K. Chen, Y.L. Zhao, Nanozymes: versatile platforms for cancer diagnosis and therapy, *Nano-Micro Lett.* 14 (2022) 95.
- M.M. Liang, X.Y. Yan, Nanozymes: from new concepts, mechanisms, and standards to applications, *Acc. Chem. Res.* 52 (2019) 2190–2200.
- X.L. Zhang, G.L. Li, D. Wu, X.L. Li, N. Hu, J. Chen, G. Chen, Y.N. Wu, Recent progress in the design fabrication of metal-organic frameworks-based nanozymes and their applications to sensing and cancer therapy, *Biosens. Bioelectron.* 137 (2019) 178–198.
- J.H. Wang, R.L. Huang, W. Qi, R.X. Su, Z.M. He, Preparation of amorphous MOF based biomimetic nanozyme with high laccase- and catecholase-like activity for the degradation and detection of phenolic compounds, *Chem. Eng. J.* 434 (2022), 134677.
- W. Wang, Q. Luo, J.Y. Li, Y.H. Li, R.G. Wu, Y.L. Li, X.B. Huo, N. Wang, Single-atom tungsten engineering of MOFs with biomimetic antibiofilm activity toward robust uranium extraction from seawater, *Chem. Eng. J.* 431 (2022), 133483.
- S. Liang, X.L. Wu, J. Xiong, X. Yuan, S.L. Liu, M.H. Zong, W.Y. Lou, Multivalent Ce-MOFs as biomimetic laccase nanozyme for environmental remediation, *Chem. Eng. J.* 450 (2022), 138220.
- F.Y. Zhang, Y.M. Li, X.M. Li, R.B. Liu, Y.X. Sang, X.H. Wang, S. Wang, Nanozyme-enabled sensing strategies for determining the total antioxidant capacity of food samples, *Food Chem.* 384 (2022), 132412.
- S. Zhao, Z.H. Xu, T. Bu, X.F. Hu, J.B. Cao, J.J. Hou, F.E. Bai, R.X. Zhang, L. Wang, G.P. Zhang, Iridium (IV) oxide-mediated microorganism nanozyme amplified immunochromatographic assay for dual-signal sensitive detection of salbutamol, *Food Control* 145 (2023), 109481.
- Z.H. Wang, X.L. Yao, Y.Z. Zhang, R. Wang, Y.W. Ji, J. Sun, D.H. Zhang, J.L. Wang, Functional nanozyme mediated multi-readout and label-free lateral flow immunoassay for rapid detection of Escherichia coli O157:H7, *Food Chem.* 329 (2020), 127224.
- L.L. Zeng, Y.X. Han, Z.W. Chen, K. Jiang, D. Golberg, Q.H. Weng, Biodegradable and peroxidase-mimetic boron oxynitride nanozyme for breast cancer therapy, *Adv. Sci.* 8 (2021), 2101184.
- Z.Y. Wang, Z.Y. Li, Z.L. Sun, S.R. Wang, Z. Ali, S.H. Zhu, S. Liu, Q.S. Ren, F. G. Sheng, B.D. Wang, Y.L. Hou, Visualization nanozyme based on tumor microenvironment "unlocking" for intensive combination therapy of breast cancer, *Sci. Adv.* 6 (2020), eabc8733.
- C.Y. Cao, N. Yang, Y. Su, Z.Y. Zhang, C.X. Wang, X.J. Song, P. Chen, W.J. Wang, X. C. Dong, Starvation, ferroptosis, and prodrug therapy synergistically enabled by a cytochrome c oxidase like nanozyme, *Adv. Mater.* 34 (2022), 2203236.
- H.J. Jeon, H.S. Kim, E. Chung, D.Y. Lee, Nanozyme-based colorimetric biosensor with a systemic quantification algorithm for noninvasive glucose monitoring, *Theranostics* 12 (2022) 6308–6338.
- M. Feng, Q. Zhang, X.F. Chen, D. Deng, X.Y. Xie, X.P. Yang, Controllable synthesis of boron-doped Zn-N-C single-atom nanozymes for the ultrasensitive colorimetric detection of p-phenylenediamine, *Biosens. Bioelectron.* 210 (2022), 114294.
- Q. Chen, B. Hu, D.D. Zhang, Q.X. Ren, M.M. Wang, P. F. Li, Y. Zhang, Transferrin guided quasi-nanocuboid as tetra-enzymic mimics and biosensing applications, *Talanta* 240 (2022), 123138.
- X.Q. Meng, D.D. Li, L. Chen, H.L. He, Q. Wang, C.Y. Hong, J.Y. He, X.F. Gao, Y. L. Yang, B. Jiang, G.H. Nie, X.Y. Yan, L.Z. Gao, K.L. Fan, High-performance self-cascade pyrite nanozymes for apoptosis-ferroptosis synergistic tumor therapy, *ACS Nano* 15 (2021) 5735–5751.
- D.M. Zhu, H. Chen, C.Y. Huang, G.X. Li, X. Wang, W. Jiang, K.L. Fan, H₂O₂ self-producing single-atom nanozyme hydrogels as light-controlled oxidative stress amplifier for enhanced synergistic therapy by transforming "cold" tumors, *Adv. Funct. Mater.* 32 (2022), 2110268.

- [36] W.Y. Zhu, G.Y. Jiang, L. Xu, B.Z. Li, Q.Z. Cai, H.J. Jiang, X.M. Zhou, Facile and controllable one-step fabrication of molecularly imprinted polymer membrane by magnetic field directed self-assembly for electrochemical sensing of glutathione, *Anal. Chim. Acta* 886 (2015) 37–47.
- [37] P. Hou, J.W. Sun, H.J. Wang, L. Liu, L.W. Zou, S. Chen, TCF-imidazo[1,5- α]pyridine: a potential robust ratiometric fluorescent probe for glutathione detection with high selectivity, *Sensor. Actuat. B Chem.* 304 (2020), 127244.
- [38] W. Yang, C.Y. Weng, X.Y. Li, H.L. He, J.W. Fei, W. Xu, X.Q. Yan, W.Y. Zhu, H. S. Zhang, X.M. Zhou, A sensitive colorimetric sensor based on one-pot preparation of h-Fe₃O₄@ppy with high peroxidase-like activity for determination of glutathione and H₂O₂, *Sensor Actuat B-Chem* 338 (2021), 129844.
- [39] G.P. McDermott, J.M. Terry, X.A. Conlan, N.W. Barnett, P.S. Francis, Direct detection of biologically significant thiols and disulfides with manganese(IV) chemiluminescence, *Anal. Chem.* 83 (2011) 6034–6039.
- [40] X. Liang, X.Z. Wang, Y.C. Zhang, B.J. Huang, L. Han, Selective inhibition toward dual enzyme-like activities of iridium nanozymes for a specific colorimetric assay of malathion without enzymes, *J. Agric. Food Chem.* 70 (2022) 3898–3906.
- [41] S.Y. He, Y. Feng, Q. Sun, Z.A. Xu, W. Zhang, Charge-switchable Cu_xO nanozyme with peroxidase and nearInfrared light enhanced photothermal activity for wound antibacterial application, *ACS Appl. Mater. Interfaces* 14 (2022) 25042–25049.